NACA

RESEARCH MEMORANDUM

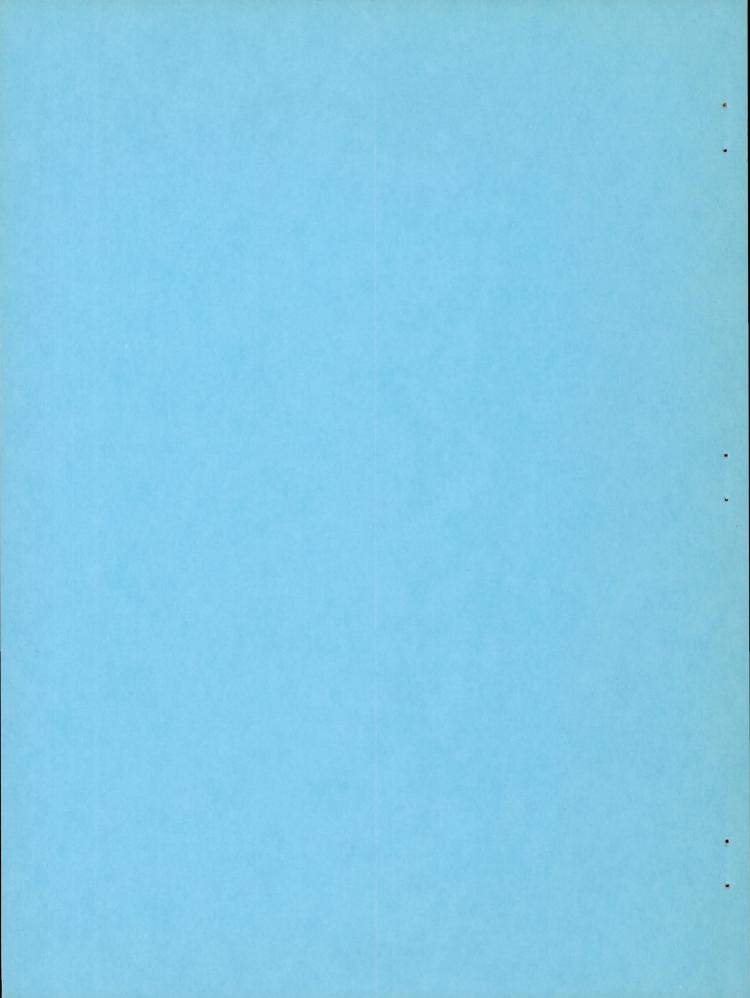
FREE-FLIGHT FLUTTER TESTS IN THE TRANSONIC AND LOW SUPERSONIC SPEED RANGE OF THREE LOW-ASPECT-RATIO, SWEPT, TAPERED WINGS ON ROCKET-PROPELLED VEHICLES By William T. Lauten, Jr., and Burke R. O'Kelly

Langley Aeronautical Laboratory
Langley Field, Va.

NATIONAL ADVISORY COMMITTEE FOR AERONAUTICS

WASHINGTON

March 19, 1956 Declassified October 31, 1958



NATIONAL ADVISORY COMMITTEE FOR AERONAUTICS

RESEARCH MEMORANDUM

FREE-FLIGHT FLUTTER TESTS IN THE TRANSONIC AND LOW SUPERSONIC SPEED RANGE OF THREE LOW-ASPECT-RATIO, SWEPT, TAPERED WINGS ON ROCKET-PROPELLED VEHICLES By William T. Lauten, Jr., and Burke R. O'Kelly

SUMMARY

Flutter data obtained by use of rocket-propelled vehicles in the transonic and low supersonic speed ranges for three low-aspect-ratio, highly tapered, swept wings are presented herein. All three wings fluttered in the transonic range.

Structural influence coefficients were obtained on each of the three plan forms, and calculated mode shapes and frequencies derived from the influence coefficients are presented.

A reference flutter speed was calculated for each configuration for the purposes of comparison and of relating the results to the results of other systematic tests. This reference flutter speed was based on a theory which includes effects of mode shape (for simplicity, only the first bending and first torsion modes were utilized) and sweep, and which involves the use of two-dimensional flutter derivatives. For the 45° and 60° swept wings the reference flutter speeds proved to be conservative by a rather large margin. The addition of a third mode to the calculations for the 60° swept wing yielded a value of flutter speed which coincided almost exactly with the experimental. For the 60° delta configuration the wing fluttered in several different modes, but in spite of the complex nature of the flutter for this configuration, the simplified reference flutter speed based on only two modes was within 5 percent of the actual speed at the beginning of flutter.

INTRODUCTION

During the last few years the Langley Aeronautical Laboratory of the NACA has been conducting a series of free-flight flutter tests utilizing freely falling bodies and rocket-propelled vehicles. They have been

Α

intended primarily to obtain information in the transonic speed range. Results of some of these tests are presented in references 1, 2, and 3. The wings have been unswept or swept with little or no taper and for the most part have had high aspect ratios. The tests reported herein utilizing rocket-propelled vehicles extend this investigation to highly tapered, low-aspect-ratio, swept wings. The plan forms tested were of 45° sweepback at the quarter-chord line, aspect ratio 3.01, taper ratio of the exposed panel of 0.2, and an NACA 65A004 airfoil section in the stream direction; 60° sweepback at the quarter-chord line, aspect ratio, taper ratio, and airfoil section the same as the above wing; and 60° delta plan form, aspect ratio 2.33, and NACA 65A003 airfoil section in the stream direction. Flutter tests in transonic tunnels of similar swept plan forms are reported in references 4 and 5. These types of wings are currently of interest to designers of future operational aircraft.

This paper presents structural data and flight-test results and a comparison of experimentally determined flutter speeds with those determined from a simplified flutter analysis based on that of reference 6.

SYMBOLS

aspect ratio (including body intercept)

a	nondimensional wing-elastic-axis position measured from midchord, positive rearward, $\frac{2x_0}{100}$ - 1
a + x _a	nondimensional wing center of gravity measured from midchord, $2x_1$
	positive rearward, $\frac{2x_1}{100}$ - 1

- b semichord of test wing normal to quarter-chord line, for models 1 and 2, in the stream direction for model 3, ft
- F calculated mode shape,

 Vertical displacement of any section

 Vertical displacement of section with maximum displacement
- f frequency, cps
- g acceleration due to gravity, 32.2 ft/sec²
- I_{α} polar mass moment of inertia about elastic axis per unit length, ft-lb-sec $^2/{\rm ft}$

mass ratio, m/πρb² Λ sweepback, deg taper ratio of exposed wing panel λ Mach number M mass of wing per unit length along c/4 for models 1 and 2 and along the semispan for model 3, slugs/ft frequency, radians/sec W air density, slugs/cu ft dynamic pressure, lb/sq ft q r_{α}^{2} square of nondimensional radius of gyration about the elastic axis, In/mb2 semispan, measured from model center line, in. S time, sec V velocity, fps VR flutter velocity derived from calculations based on twodimensional, incompressible-flow theory of reference 6 distance of elastic axis of wing section behind leading edge, XO measured perpendicular to the quarter-chord line for models 1 and 2, in the stream direction for model 3, percent chord distance of center of gravity of wing section behind leading X7 edge, measured perpendicular to the quarter-chord line for models 1 and 2, in the stream direction for model 3, percent chord Subscripts:

е	experimental	values	obtained	at	the	start	of	sustained	flutter

calculated values based on two-dimensional, incompressibleflow theory of reference 6

first bending h

second bending ha

α₁ first torsion

f flutter frequency at any indicated time

stnd. at standard conditions

MODELS AND INSTRUMENTATION

Test Wings

Dimensioned drawings of the plan forms of the three test models are shown in figure 1. The wings were made of laminated spruce; the direction of the grain of the center lamination was streamwise and that of the outer laminations was parallel to the quarter-chord line, except for model 3 where the grain of the outer laminations extended fanwise from the tip.

The wings of model 1 were swept back 45° at the quarter-chord line and had an aspect ratio of 3.01, a taper ratio of the exposed panel of 0.2, and NACA 65A004 airfoil section in the stream direction.

The wings of model 2 were swept back 60° at the quarter-chord line and had the same aspect ratio, taper ratio, and section as the wings of model 1.

The wings of model 3 were 60° delta plan forms with a tip radius which removed an area from each panel equal to one-eighth of one percent of the total wing plan form. The aspect ratio was 2.33 and the airfoil section was NACA 65A003 in the stream direction.

Table I gives various physical characteristics of all the wings. The positions of the elastic axis \mathbf{x}_0 and of the wing center of gravity \mathbf{x}_1 were assumed to be as listed in the table on the basis of the particular wing airfoil section.

General Configuration

Each model consisted of a 5-inch cordite rocket motor (which served as the major portion of the fuselage), a telemeter housed in a nose section at the forward end of the rocket motor, and an assembly made of plates welded to a magnesium sleeve which slipped over the rear end of the rocket motor. The test wings were attached to this assembly. The general model arrangement is shown in figure 2 which is a sketch of model 2. A photograph of model 1 is shown as figure 3(a).

Model 1 was boosted to a Mach number of 0.75 by a lightweight HVAR rocket motor. The other models were boosted to a Mach number of 1.15 by lightweight HVAR rocket motors one and one-half the original length. After separation of a model from its booster, the rocket motor of the model ignited and carried it to the highest Mach numbers obtained in the test. A photograph of model 3 with its booster on the rail launcher is shown in figure 3(b). Weight and balance data for the models are shown in table II.

Instrumentation

The models were equipped with telemeters which gave continuous records of the quantities to be measured. These quantities for all models were right wing bending and torsional oscillations derived from strains detected by strain gages mounted near the root of the wing. In addition, for model 2 total and static pressures were measured.

Atmospheric conditions prevailing at the times of the flights were obtained from radiosondes. Each radiosonde was tracked by radar during its ascent to determine the wind direction and velocity. Two radar sets tracked the models during their flights; one to give velocity of the models with respect to a ground reference point and the other to give their positions in space. All models were tracked by motion-picture cameras to give photographic records of the flights. The models were launched at the Langley Pilotless Aircraft Research Station at Wallops Island, Va.

Ground Tests

Prior to the flight tests, the wings of the models were vibrated in the laboratory to determine their natural frequencies and nodal patterns. Results of these tests are shown in figure 4. Various physical characteristics of the wings are listed in table I. The elastic axis position is assumed on the basis of section characterisites. All other quantities are measured.

The structural influence coefficients of the wing panels were measured with dial gages which could be read to 10^{-14} inches. The panels were loaded by means of a weighted frame which could be slipped over the wing in such a manner that a point load could be applied. Tables III, IV, and V present the influence coefficients along with a sketch showing the points of load application and a column giving the mass of the segments of the wing associated with the influence coefficients. In the case of model 3 the wing on which the influence coefficients were determined was a test panel which was not flown. However, its frequencies compare favorably with the frequencies of the flight-tested wings, and

it is believed that the mode shapes should compare even more favorably since the mode shape is more nearly a function of plan form than of stiffness.

The influence coefficients and the masses of the segments were used to form dynamic matrices from which, by a method of matrix iteration illustrated in reference 7, the natural mode shapes and associated frequencies for first bending and first torsion modes were calculated. In addition the second bending mode was calculated for models 2 and 3. These mode shapes and frequencies are tabulated in table VI. The calculated frequencies compare favorably with the values obtained experimentally. The mode shapes were not measured experimentally but the node lines determined from the calculated mode shapes (table VI) seem to be in reasonable agreement with the experimentally determined node lines (fig. 4).

RESULTS

Experimental results and calculated flutter speeds and frequencies for the right wing of each model are presented in table VII. Figure 5 shows the variation of velocity, Mach number, and density with time for each model; and figure 6 shows portions of the telemeter records of each model.

Model 1.- A time history of the flight of model 1 showing Mach number, velocity, and atmospheric density is shown in figure 5(a); and a portion of the telemeter record showing the flutter oscillations of the right wing is shown in figure 6(a). These figures show flutter beginning at 3.69 seconds at M = 1.142 at a frequency of 142 cps. This flutter continued up to about 5.62 seconds (M = 1.61, $f_f = 160$ cps), where a low-amplitude, short-period oscillation of the model occurred and the flutter damped out temporarily. The flutter began again at 5.99 seconds (M = 1.68, $f_f = 165$ cps), continued through the maximum Mach number of the test (M = 1.78, $M_f = 167$ cps), and on to 8.14 seconds (M = 1.435, $M_f = 144$ cps) where flutter stopped.

Model 2.- A time history of the flight of model 2 showing Mach number, velocity, and atmospheric density is shown in figure 5(b) and a portion of the telemeter record showing the flutter oscillations of the right wing is reproduced in figure 6(b). This wing experienced two bursts of low-amplitude oscillations, (not shown on fig. 6(b)), the first just after separation from the booster at M = 1.007 and the second at M = 1.005. Figure 6(b) shows sustained flutter beginning at about 2.6 seconds (M = 1.15, $f_f = 156$ cps). These oscillations damped out at about 3.45 seconds (M = 1.43, $f_f = 160$ cps) and began again at 3.55 seconds (M = 1.43, $f_f = 132$ cps). The fact that in the second burst of sustained flutter the frequency decreased to 132 cps indicates

that the mode of the flutter had changed, since ordinarily the frequency tends to increase with increase in Mach number as in the test of model 1. The wing continued to flutter and the frequency continued to decrease up to 4.82 seconds (M = 1.75, $f_f = 118$ cps) when the signal from the strain-gage telemeter channels failed. It is believed that the wings did not fail since the model exhibited no tendency to become unstable during the remainder of the flight.

Model 3. - The time history of the flight of model 3 showing Mach number, velocity, and atmospheric density is shown in figure 5(c). A portion of the telemeter record is reproduced in figure 6(c) and shows the signal from the right wing bending and torsion strain gages. Incipient flutter started at about 0.83 second (not shown in figure 6(c)) at a Mach number of 0.72 with a frequency of 184 cps. This frequency changed to 271 cps and after booster separation, the oscillations damped out as the model slowed down. As may be seen in figure 6(c), at about 1.73 seconds, when the sustainer rocket in the model had been burning about 0.1 second, the flutter began again at a frequency of 266 cps (M = 0.96). This oscillation in turn almost stopped and then started again as relatively sustained flutter at M = 1.08 at a frequency of 276 cps. This flutter continued up to about 2.7 seconds, ff = 280 cps, where the characteristics of the oscillations changed and a beat frequency of 40 cps became evident on the torsional strain-gage channel while the high frequency continued. There is also evident a short-period stability oscillation of the model which continued until about 4.45 seconds. At 3.15 seconds (M = 1.41) the flutter frequency had decreased to 238 cps, and subsequently the beat gradually disappeared until at 3.4 seconds it was no longer in evidence. The flutter continued with gradually decreasing frequency until at 4.4 seconds (M = 1.73) the frequency was 203 cps and the oscillations were temporarily reduced in amplitude. The amplitude immediately built up again at a frequency of 227 cps and again a change in the characteristics of the flutter is evident with a beat frequency of 33 cps becoming apparent on the bending strain-gage channel. This mode of flutter continued until 5.7 seconds (M = 1.96) when the signal from the strain-gage telemeter channels failed. Other records of the flight indicate that the wings did not fail.

DISCUSSION

In order that the results may be compared with previous tests as readily as possible, a theoretical, or reference, flutter speed $V_{\rm R}$ was calculated by the method of reference 6; that is to say, calculated on the basis of two-dimensional flow (strip analysis) with the effect of mode shape and the angle of sweep included. Aerodynamic coefficients for two-dimensional incompressible flow were employed in conjunction with

two degrees of freedom. The frequencies used were the frequencies obtained in the vibration tests of the wings. The air density used was that at the start of sustained flutter. Section parameters of the 45° and 60° swept wings were taken perpendicular to the quarter chord, whereas for the 60° delta wing the streamwise section was used. The sweep angle of the quarter-chord line was used in the calculations for the 45° and 60° swept wings; the sweep angle of the leading edge was used in the calculations for the 60° delta wing. The reference flutter speed calculation should not be expected to predict accurately an experimental flutter speed. Rather it may be considered as a least common denominator which serves to eliminate in part the effect of certain wing parameters in order that a figure such as figure 7 can be made more general.

Figure 7, a plot of V/V_R and V_e/V_R against Mach number, presents flutter information obtained in this investigation and, for the purpose of comparison, some data from a previous investigation of swept, tapered wings (ref. 2). With reference to the present tests, the beginning of flutter is shown by the open symbol and the lines extending from these points show the flutter range of V/V_R . It may be seen from the figure that the reference flutter speed is quite conservative in the case of models 1 and 2, much more so than for the wings reported in reference 2 which had a taper ratio of 0.52 and aspect ratios of 4.25 and 8 for the 60° and 45° swept wings, respectively. In the case of model 3, the delta plan form, the calculated speed is slightly unconservative.

In the case of model 1 the flutter behavior is essentially straightforward and, in view of the assumptions made in order to simplify the calculations, the agreement between theory and experiment may be considered reasonable ($V_{\rm e}/V_{\rm R}=1.33$).

For model 2 the flutter behavior is more involved since the wing apparently fluttered in two modes. Two calculations of flutter speed were made. In the first calculation only the first bending and first torsion modes were used. The result was a calculated flutter speed which was conservative by a factor of approximately 2. In addition, the flutter frequency derived from the calculation was much lower than the experimental, and just slightly more than the first bending $(f_f/f_{h_1} = 1.129)$. Since this frequency was considerably less than the experimental value, it was decided that a calculation involving an additional mode, second bending, should be made. This calculation yielded a value for the flutter velocity which was very close to the experimental value ($V_e/V_R = 1.01$). In addition, the frequency derived from the calculations involving the three modes was in considerably better agreement with the value obtained experimentally ($f_e/f_R = 1.32$). The fact that V_R was more than doubled was unexpected since previous experience has indicated that flutter velocities calculated for wings of this sweep are not exceptionally sensitive to the addition of the third mode. For example, reference 4, in calculations for a 60° swept, aspect-ratio-4 wing, shows a change

in V_R of only 30 percent between calculated flutter velocities where two and three modes were used. Reference 5 reports a negligible difference from the addition of the third mode in the case of a 45° swept, aspect-ratio-3.3 wing. It is interesting to note that in reference 4 the addition of the third mode caused a decrease in V_R , while in the case of model 2 reported herein V_R showed a marked increase. An important aspect is that in both cases, that is, from reference 4 and model 2, the agreement with the experimental values was improved. A possible explanation for the marked effect obtained on model 2 is that the wing fluttered at frequencies (156 and 133 cps) which are near the second bending frequency (148 cps), and the flutter could be strongly influenced by the second bending mode. For the three mode calculations the ratio V_e/V_R obtained from the tests in the transonic tunnel reported in reference 4 is in good agreement with the same ratio obtained from the free-flight rocket test of model 2.

In the case of model 3 it is obvious from the flutter record that the flutter behavior is complex. From the beginning of the first short burst until the signal from the strain gages failed some 5 seconds later, there are five distinct types of oscillation as indicated by either an abrupt change in frequency (from 203 cps to 227 cps in about 0.05 second), abrupt changes in amplitude, a change in the characteristics of the strain-gage signals (such as a change from a beat frequency on the torsion gage to a beat frequency on the bending gage), or combinations of the three. These different types of oscillation might well be referred to as different modes of flutter. A point of interest is that for only two very brief periods of time (t = 0.82 and 4.4 seconds) did the frequency of oscillation drop below that of the second natural mode - torsion, 215 cps. In the initial portion of the sustained flutter, the frequency was above that of the third natural mode - second bending, 258 cps. The fourth natural mode occurred at a frequency of 420 cps and apparently involves camber of the airfoil section. This flutter in apparently random modes has previously been observed during delta wing flutter reported in reference 8 when wings fluttered at several distinctly different frequencies which fell at random between the frequencies of the first and fourth natural modes of the models.

The calculated flutter velocity yields a ratio $V_{\rm e}/V_{\rm R}=0.965$. The close agreement between calculations and experiment is somewhat surprising in view of the complex nature of the flutter of this model and the simplified type of analysis performed. As stated previously, the sections considered for the mass and inertia parameters were the streamwise section, and the mode shape was taken perpendicular to the free stream so that in these respects the sweep angle of the leading edge did not enter into the calculations. On the other hand, in the various aerodynamic terms of the flutter-determinant elements where the sweep angle was required, the sweep angle of the leading edge was employed. After the

flutter speed coefficient $V/b\omega_{CL}$ was solved for the velocity V, the reciprocal of the cosine of the leading-edge sweep angle was used as a multiplying factor to obtain the value of V_R listed in table VII. In view of the method utilized in obtaining the answer such agreement between calculations and experiment must be considered largely fortuitous.

CONCLUDING REMARKS

Flutter has been obtained in the transonic range with three low-aspect-ratio, highly tapered, swept wings at speeds, which for the 45° and 60° swept wings, exceed by a large margin values obtained from calculations which employ incompressible, two-dimensional-flow flutter derivatives and the first natural bending and torsion modes. In the case of the 60° delta wing the calculated speed compared favorably with the experimental speed. In the case of the highly tapered 60° swept wing the addition of the third mode (second bending) to the calculations reduced the margin between the calculated and experimental values by a marked amount. The flutter records obtained from the test of the 60° delta plan form indicate that this type of wing can be expected to flutter in higher modes than the more beam-like swept wings.

Langley Aeronautical Laboratory,
 National Advisory Committee for Aeronautics,
 Langley Field, Va., November 14, 1955.

REFERENCES

- 1. Lauten, William T., Jr., and Teitelbaum, J. M.: Some Experiments on the Flutter of Wings With Sweepback in the Transonic Speed Range Utilizing Rocket-Propelled Vehicles. NACA RM L50C03a, 1950.
- 2. Lauten, W. T., Jr., and O'Kelly, Burke R.: Results of Two Experiments on Flutter of High-Aspect-Ratio Swept Wings in the Transonic Speed Range. NACA RM L52D24b, 1952.
- 3. Lauten, W. T., Jr., and Sylvester, Maurice A.: Flutter Investigation of Two Thin, Low-Aspect-Ratio, Swept, Solid, Metal Wings in the Transonic Range by Use of a Free-Falling Body. NACA RM L51K28a, 1952.
- 4. Unangst, John R., and Jones, George W., Jr.: Some Effects of Sweep and Aspect Ratio on the Transonic Flutter Characteristics of a Series of Thin Cantilever Wings Having a Taper Ratio of 0.6.

 NACA RM 155113a, 1955.
- 5. Maier, H. G., and King, S. R.: Special Progress Report. The Critical Flutter Mach Number for 45° Sweptback Wings Transonic Flutter Model Test. Rep. No. C.A.L.-70, (Contract No. AF 33(616)-199), Cornell Aero. Lab., Inc., Jan. 1955.
- 6. Barmby, J. G., Cunningham, H. J., and Garrick, I. E.: Study of Effects of Sweep on the Flutter of Cantilever Wings. NACA Rep. 1014, 1951. (Supersedes NACA TN 2121.)
- 7. Scanlan, Robert H., and Rosenbaum, Robert: Introduction to the Study of Aircraft Vibration and Flutter. The Macmillan Co., 1951, pp. 168-186.
- 8. Herr, Robert W.: A Preliminary Wind-Tunnel Investigation of Flutter Characteristics of Delta Wings. NACA RM L52B14a, 1952.

TABLE I.- WING PARAMETERS

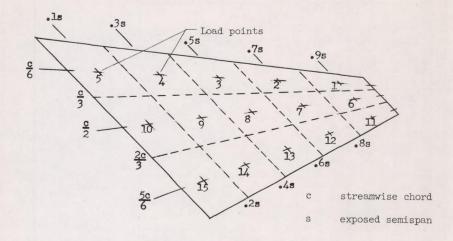
	Mode	el l	Mode	el 2	Mode	1 3
	Left semispan	Right semispan	Left semispan	Right semispan	Left semispan	Right semispan
Airfoil section \dots λ \dots λ \dots \dots μ_{stnd} \dots	65A004 19.12 .2 15.53 38 35 -0.300 -0.240 0.1819 83	65A004 19.12 .2 15.64 36.6 35 -0.300 -0.268 0.1833 85	65A004 19.12 .2 20.8 34.5 35 -0.300 -0.310 0.194 40.5	65A004 19.12 .2 22.4 34.4 35 -0.300 -0.312 0.208 44	65A003 17.28 0 14.2 44.9 40 -0.200 -0.102 0.195 130	65A003 17.28 0 13.7 44.7 40 -0.200 -0.106 0.195 116
f _{h2} , cps	244	248	135	148.5	287	259
f_{α_1} , cps	206	201	196	197	238	221
A	3	.01	3	.01	2.	33

TABLE II.- MASS BALANCE CHARACTERISTICS OF MODELS

	Model 1	Model 2	Model 3
Weight with fuel, lb	87.5	93.0	94.0
	60.0	65.4	66.0
	44.9	47.6	45.7
	44.5	46.8	40.65

TABLE III. - STRUCTURAL INFLUENCE COEFFICIENTS OF MODEL 1 WING
AT LOAD POINTS INDICATED IN SKETCH

[10-pound load]



Segment (a)	Mass, (lb-sec ² /in.)	Segment (a)	Mass, (lb-sec ² /in.)
1 2 3 4 5 6 7	3.90 × 10 ⁻⁵ 9.30 16.96 26.80 38.90 5.04 12.00	8 9 10 11 12 13 14 15	21.90 × 10-5 34.90 50.30 2.13 5.06 9.27 14.65 21.20

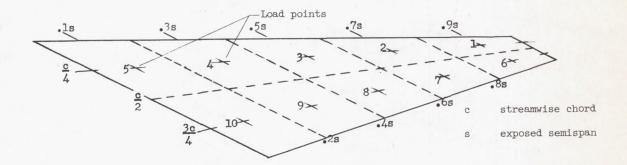
 ${\tt aSegments}$ are identified by numbers within separating lines in sketch.

Load		Deflection, in. \times 10 ⁴ , at load points -													
points	1	2	3	4	5	.6	7	8	9	10	11	12	13	14	15
1 2 3 4 5 6 7 8 9 10 11 12 13 14 15	2,047 772 3333 111 14 1,435 750 334 121 1,210 584 233 59 9	779 551 273 96 14 676 434 221 88 10 574 311 129	326 264 202 78 12 276 198 112 46 8 224 130 53 10	96 83 73 51 9 79 56 36 14 1 54 34 11 0	14 14 13 12 10 11 9 6 2 0 6 4 1	1,429 661 263 72 9 1,548 765 346 113 12 1,548 766 320 87	739 429 191 59 7 7777 506 255 90 12 802 506 243 76	334 221 115 39 5 346 252 161 56 9 350 255 145 51	108 75 38 10 0 112 81 57 30 2 102 82 50 16	14 11 5 2 0 15 12 8 5 3 14 11 8 2	1,194 530 217 58 6 1,521 771 323 92 12 2,114 979 424 106	570 285 119 35 4 751 491 242 77 11 972 864 420 126 13	229 113 47 11 0 318 235 138 52 7 414 417 380 141	59 25 7 1 0 93 72 45 18 2 124 139 149 143 23	3 0 0 0 0 7 6 4 1 0 12 15 18 24 26

TABLE IV. - STRUCTURAL INFLUENCE COEFFICIENTS OF MODEL 2 WING

AT LOAD POINTS INDICATED IN SKETCH

10-pound load



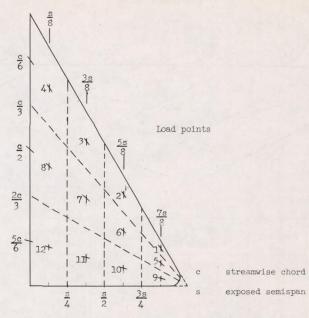
Segment (a)	Mass, (lb-sec ² /in.)	Segment (a)	Mass, (lb-sec ² /in.)
1	7.2254 × 10-5	6	5.1224 × 10 ⁻⁵ 11.9785 21.3037 32.5375 45.4082
2	16.8961	7	
3	30.7392	8	
4	45.8979	9	
5	64.0532	10	

 $^{\rm a} \rm Segments$ are identified by numbers within separating lines in sketch.

Load		Deflection, in. × 10 ⁴ , at load points -													
points	1	2	3	4	5	6	7	8	9	10					
1 2 3 4 5 6 7 8 9	3,686 1,851 730 196 6 3,906 2,245 1,072 357 32	1,850 1,194 541 159 11 1,852 1,264 684 247	772 562 344 122 9 744 546 331 135	216 171 121 69 9 194 150 93 39	14 14 11 8 5 12 10 5 2	3,950 1,869 762 196 4,826 2,602 1,230 435 36	2,230 1,244 543 148 5 2,568 1,781 931 352 36	1,076 680 330 95 4 1,220 936 618 261 34	380 254 138 42 2 432 352 259 159 25	50 35 21 7 0 60 49 39 29					

TABLE V.- STRUCTURAL INFLUENCE COEFFICIENTS OF MODEL 5 WING $\mbox{AT LOAD POINTS INDICATED IN SKETCH}$

[10-pound load]



Segment (a)	Mass, (lb-sec ² /in.)	Segment (a)	Mass, (lb-sec ² /in.)		
1 2 3 4 5 6	1.9349 × 10-5	7	27.3850 × 10-5		
	8.5055	8	46.0557		
	21.0249	9	1.6597		
	38.1720	10	5.8096		
	2.9080	11	12.4482		
	11.6176	12	21.5755		

 $\ensuremath{^{\mathrm{a}\mathrm{Segments}}}$ are identified by numbers within separating lines in sketch.

Load		Deflection, in. × 104, at load points -													
points	1	2	3	4	5	6	7	8	9	10	11	12			
1	2,130	446	82	4	1,806	554	144	16	1,400	440	122	12			
2	458	405	100	7	366	221	82	11	265	93	18				
3	77	101	103	11	63	39	24	5	49	15	1				
4	4	11	11	11	2	1	1	Ó	1	Ó	0	(
5	1,846	348	60	2	1,964	572	140	16	2,142	742	200	11			
6	568	223	46	3	561	311	93	12	558	292	97	10			
7.	140	76	23	1	140	94	56	9	135	80	30	1			
8	15	11	3	0	8	6	7	5	7	5	2	(
9	1,408	268	40	4	2,040	542	134	14	3,320	1,052	286	31			
10	450	62	6	0	700	260	. 76	0	1,028	970	316	40			
11	113	9	0	0	190	96	27	3	292	314	323	51			
12	10	1	0	0	15	4	2	0	30	37	48	45			

TABLE VI.- CALCULATED MODE SHAPES AND FREQUENCIES

(a) Model 1, right wing

(b) Model 2, right wing

(c) Model 3, sample wing

Reference load point (table III)	F _h 1	Fal
1	1.0000	-0.9410
2	.4873	4333
3	.2255	4042
4	.0706	1880
5	.0103	0313
6	.9102	0425
7	.5290	.0676
8	.2578	.0587
9	.0876	0023
10	.0117	.0021
11	.9208	.7278
12	-5341	1.0000
13	.2547	.8545
14	.0791	.4031
15	.0079	.0595
fcalculated, cps fmeasured, cps	90.32	202.9

Reference load point (table IV)	Fhl	F _{h2}	F_{α_1}
1	0.9068	-0.5579	-0.9211
2	.5074	.2807	-1.0000
3	.2270	.3799	6430
4	.0656	.1844	3501
5	.0031	.0229	0555
6	1.0000	-1.0000	.6169
7	.6357	0111	.9302
8	.3370	.3097	.9668
9	.1271	.2228	.6982
10	.0135	.0449	.1244
fcalculated, cps fmeasured, cps	49.8	156.4 148.5	195.8 197

Reference load point (table V)	Fhl	F_{α_1}	F _{h2}	
1	0.7804	1.0000	-0.3465	
2	.2216	.6027	.4963	
3	.0470	.1962	.2340	
4	.0020	.0141	.0196	
5	.8855	.3902	6176	
6	.3158	.2001	.2426	
7	.0900	.0785	.1562	
8	.0072	.0150	.0232	
9	1.0000	3560	-1.0000	
10	.4526	9802	.2033	
11	.1597	6374	.3868	
12	.0175	1085	.0712	
fcalculated, cps fmeasured, cps	115.2	204.3	254 275	

TABLE VII. - EXPERIMENTAL FLUTTER DATA FOR RIGHT WINGS

Parameter	Model 1	Model 2		W-1-7-7
rarameter		2 modes	3 modes	Model 3
M _e	1.142	1.15		0.98
V _e , fps	1242	1295		1105
f _e , cps	142	156		266
ρ _e , slugs/cu ft	0.00236	0.00221		0.00277
qe, lb/sq ft	1820	1853		1386
μ _e	15.78	24.15		14.51
V _R , fps	920	583.5	1281	1146.3
f _R , cps	216.4	50.2	118.2	199.8
v_e/v_R	1.33	2.22	1.003	0.965

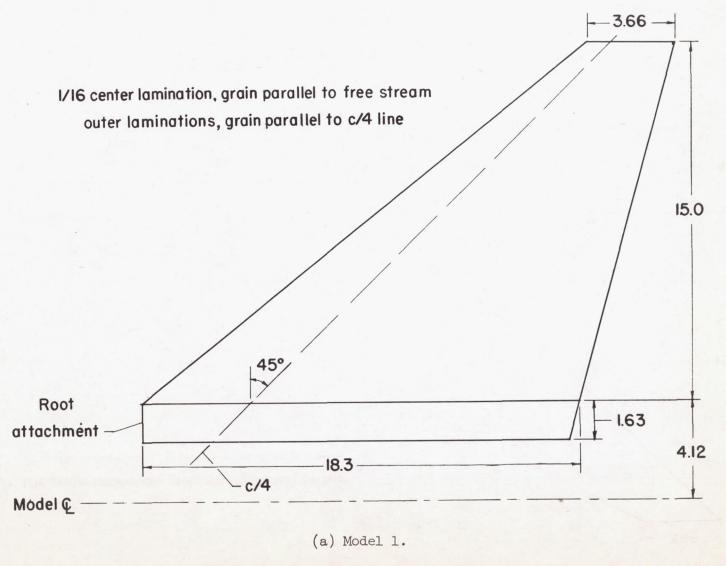
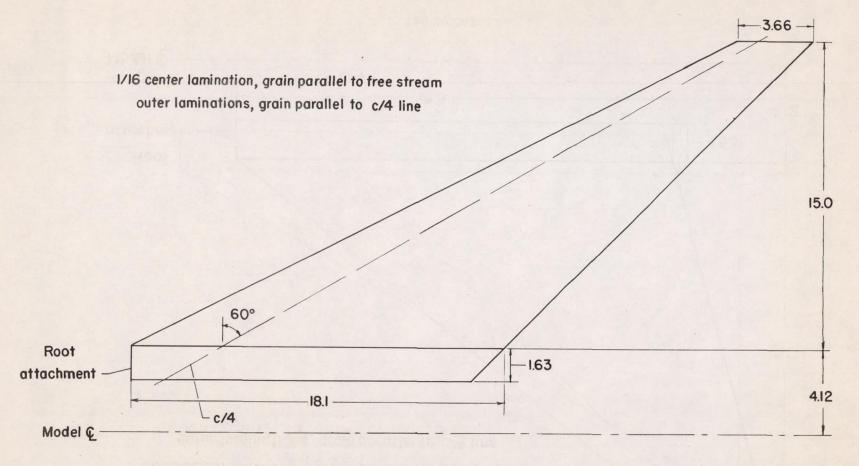


Figure 1.- Sketches of the wings.



(b) Model 2.

Figure 1.- Continued.

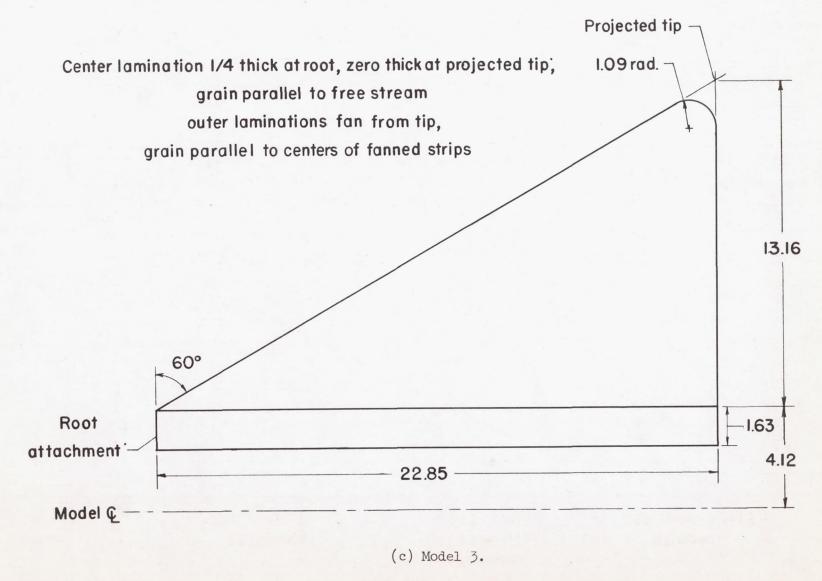


Figure 1.- Concluded.

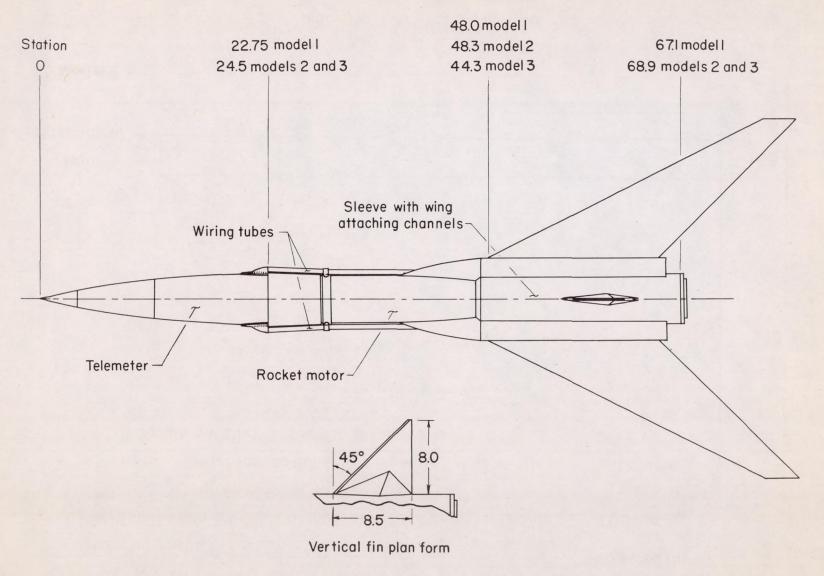
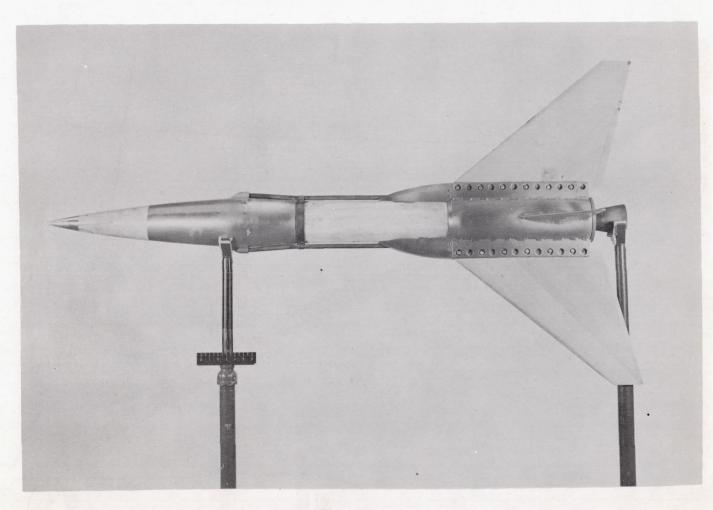


Figure 2.- General model arrangement. All dimensions are in inches.



(a) Model 1.

Figure 3.- Photographs of the models.

L-78040.1



(b) Model 3 and booster on launcher. L-82350
Figure 3.- Concluded.

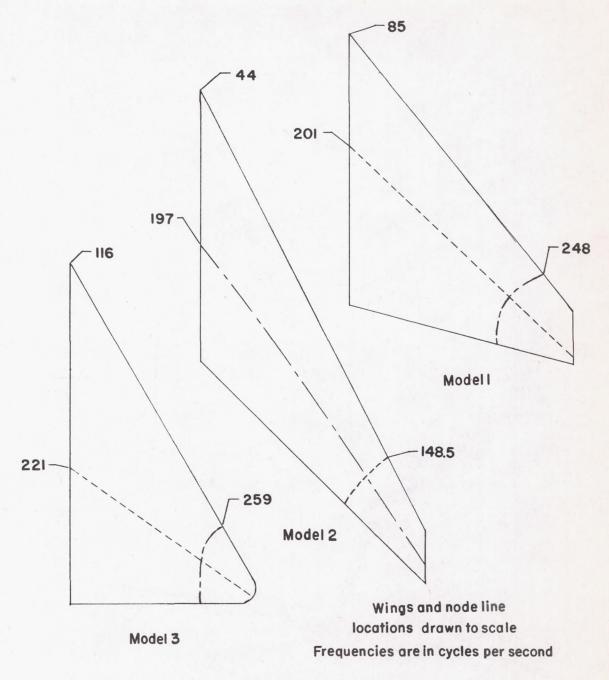


Figure 4.- Nodal patterns of right wings for first three modes of vibration.

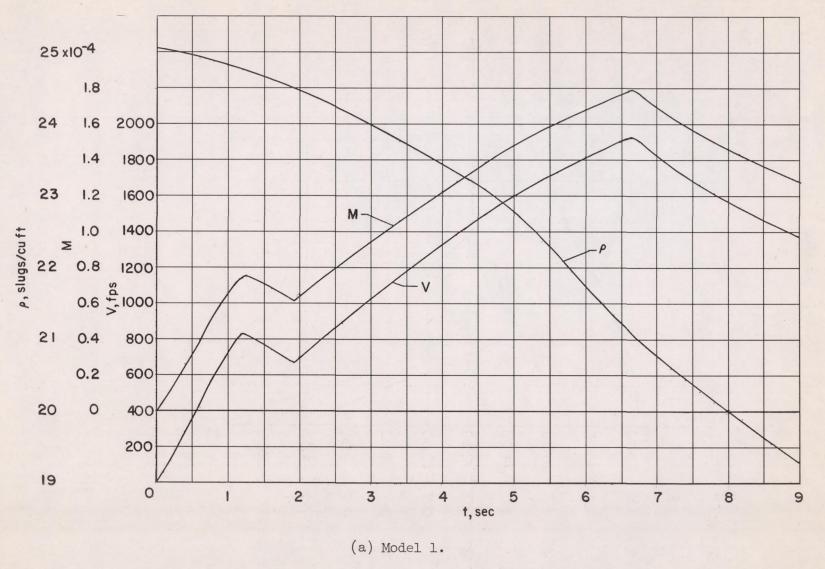
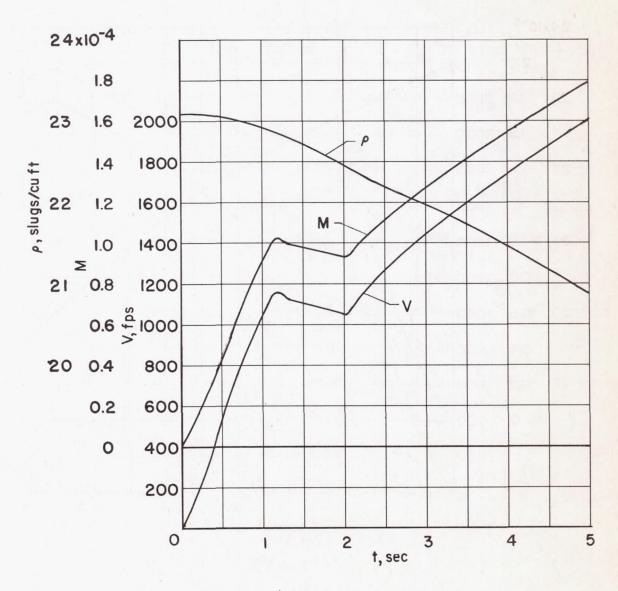
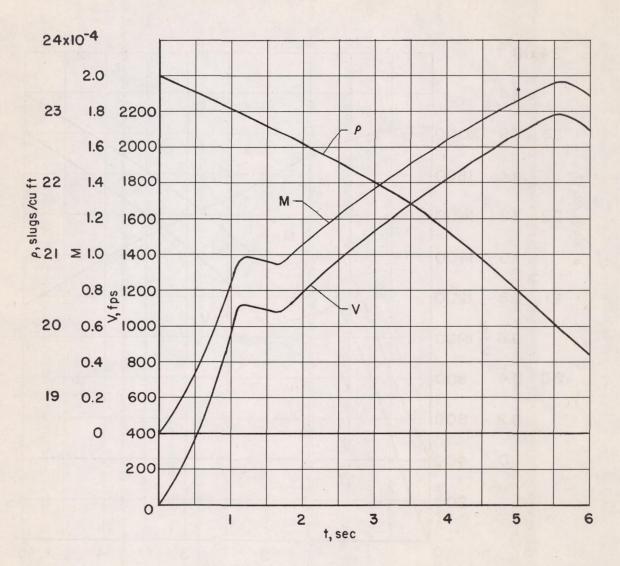


Figure 5.- Time histories showing Mach number, velocity, and air density.



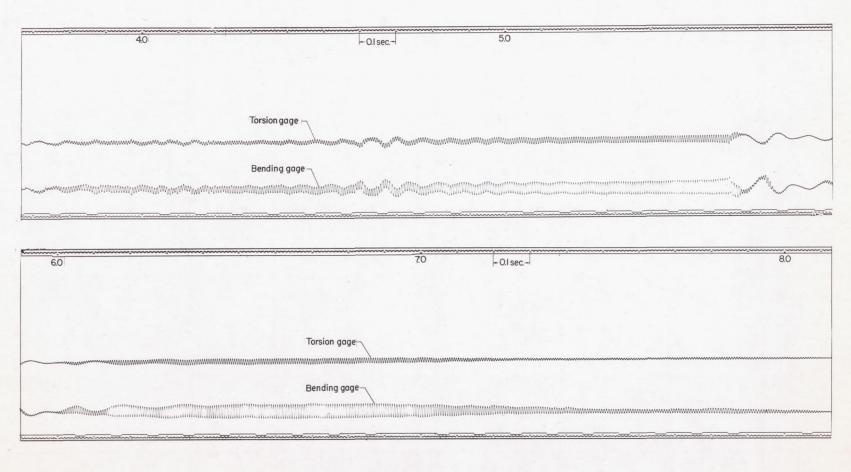
(b) Model 2.

Figure 5.- Continued.



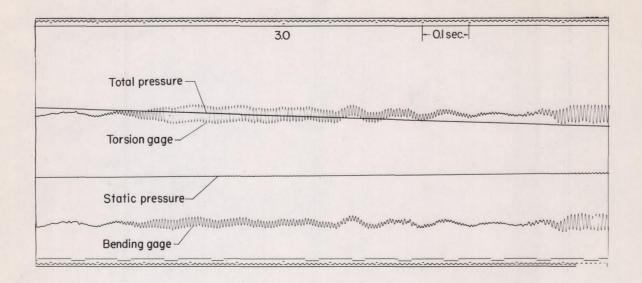
(c) Model 3.

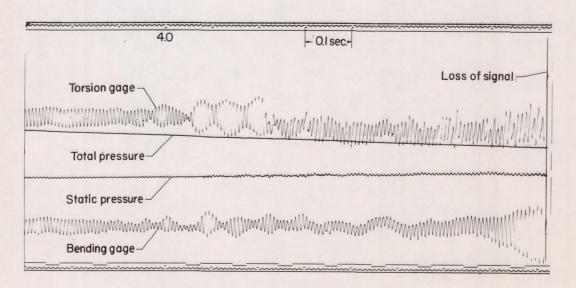
Figure 5.- Concluded.



(a) Model 1.

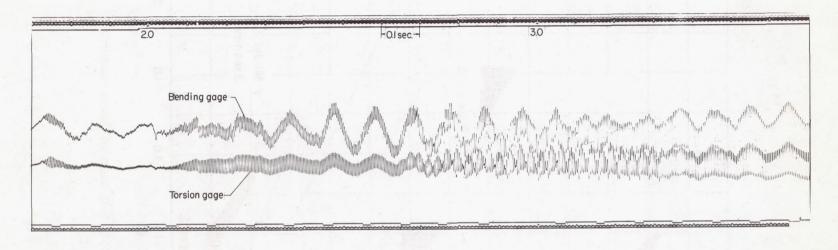
Figure 6.- Portions of the telemeter records.

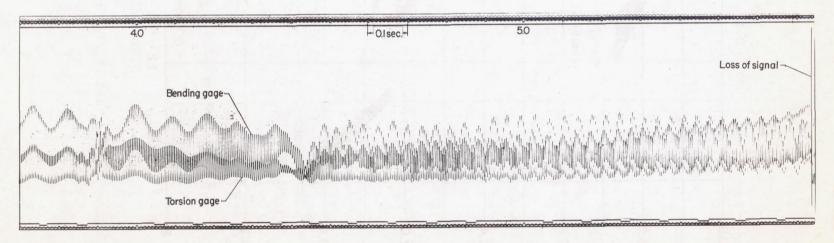




(b) Model 2.

Figure 6.- Continued.





(c) Model 3.

Figure 6.- Concluded.

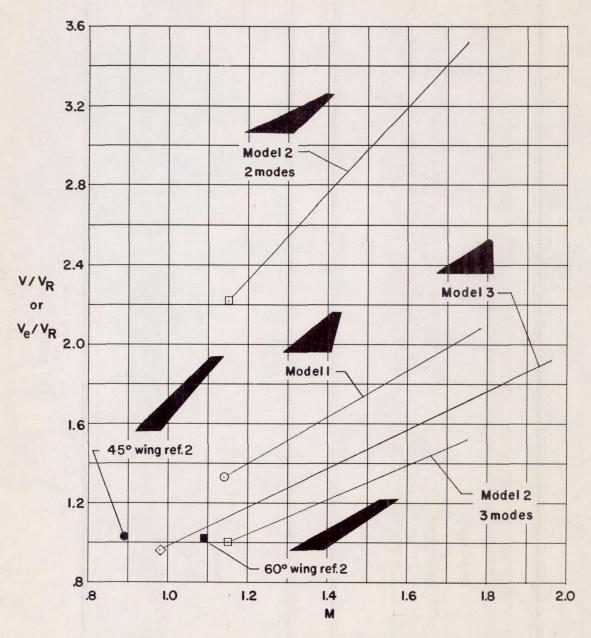


Figure 7.- V/V_R and V_e/V_R as a function of Mach number.